INTERNATIONAL JOURNAL OF NUMERICAL MODELLING: ELECTRONIC NETWORKS, DEVICES AND FIELDS
Int. J. Numer. Model. 2012; **25**:490–511
Published online 7 March 2012 in Wiley Online Library (wileyonlinelibrary.com). DOI: 10.1002/jnm.1827

Nystrom-type techniques for solving electromagnetics integral equations with smooth and singular kernels

M. V. Balaban*,†, E. I. Smotrova, O. V. Shapoval, V. S. Bulygin and A. I. Nosich

Institute of Radiophysics and Electronics NASU, Kharkiv 61085, Ukraine

SUMMARY

Considered are the problems of electromagnetic wave scattering, absorption and emission by several types of two-dimensional and three-dimensional dielectric and metallic objects: arbitrary dielectric cylinder, thin material strip and disk, and arbitrary perfectly electrically conducting surface of rotation. In each case, the problem is rigorously formulated and reduced to a set of boundary integral equations with smooth, singular and hyper-singular kernel functions. These equations are further discretized using Nystrom-type quadrature formulas adapted to the type of kernel singularity and the edge behavior of unknown function. Convergence of discrete models to exact solutions is guaranteed by general theorems. Practical accuracy is achieved by inverting the matrices of the size that is only slightly greater than the maximum electrical dimension of corresponding scatterer. Sample numerical results are presented. Copyright © 2012 John Wiley & Sons, Ltd.

Received 31 July 2011; Revised 14 October 2011; Accepted 23 November 2011

KEY WORDS: integral equations; method of analytical regularization; eigenvalue problem; generalized boundary conditions

1. INTRODUCTION

The problems of electromagnetic wave scattering, if considered as boundary-value problems for the Maxwell (in 3-D) or Helmholtz (in 2-D) equations, can be reduced to various boundary integral equations (IEs) [1]. This should be performed properly because otherwise the equivalency to original problem can be lost that entails the loss of uniqueness and existence as it happens, for example, with ‘spurious resonances’ in the scattering by perfectly electrically conducting (PEC) and dielectric bodies [2].

Even if this is avoided, the obtained IEs are always singular because of the nature of kernel functions, which are the Green’s functions and their derivatives. Therefore, the discretization of electromagnetic IEs is non-trivial task, although associated difficulties are sometimes ignored by the researchers without a solid mathematical background. Those who have such a background elegantly label this problem ‘dense-mesh breakdown’ and try to devise pre-conditioners that somehow improve the considered IEs [3]. An ideal pre-conditioner must convert a ‘bad’ IE into a ‘good’ one, amenable to trusted numerical solution. The best is to convert the problem to a Fredholm IE of the second kind (FIE-2) because these equations can be solved with any non-pathological discretization scheme. This is because the convergence, understood in proper mathematical sense as a possibility to minimize the error of computations by solving progressively larger matrix equations, is guaranteed by general theorems [1,4]. There is a special approach termed method of analytical regularization (MAR) aimed at the analytical inversion of the most singular parts of IEs [5]. On such inversion, the resulting IE is automatically an FIE-2. Sometimes, it is possible to combine analytical regularization and discretization in one operation. For instance, this is the case when the set of orthogonal eigenfunctions of the most singular operator is available and used as a full projection basis in a Galerkin discretization.

*Correspondence to: M. V. Balaban, Institute of Radiophysics and Electronics NASU, Kharkiv 61085, Ukraine.
†E-mail: mikhail.balaban@gmail.com

Still the direct numerical solutions to electromagnetic IEs are attractive because of simplicity of implementation. Fortunately, the question of whether it is possible to avoid pre-conditioning and still build an algorithm with guaranteed convergence has positive answer. The key is the idea of Nystrom, dating from the 1930s, of the use of interpolation polynomials and highest algebraic accuracy quadrature formulas for calculation of various integrals. A further milestone was the observation that such formulas could be derived in such a way that they take account of singular or even hyper-singular character of the integrand functions [6–8]. Additionally, the (possibly singular) behavior at the endpoints, if the integration contour is an open arc, can be also incorporated. All these, together with proven convergence, have already lead to creation of new economic and accurate tools for computer-aided analysis and synthesis in electromagnetics [9,10]. There are only a few points where the MAR-based techniques clearly outperform Nystrom-type methods. For instance, with the latter the derivation of approximate analytical solutions is not possible, while with the former this can be performed in the form of asymptotic series in the powers of small parameter, whose tending to zero makes the continuous operator in FIE-2 vanishing. Besides, only discrete versions of FIE-2 can be reliably solved by using iterative numerical methods instead of matrix inversion, because they provide the convergence of iterations. This can be attractive for electrically very large scatterers where direct inversions with both MAR and Nystrom algorithms are time consuming.

Our paper reports on the recent progress in the development and implementation of the Nystrom-type techniques used to build convergent and economic algorithms of numerical solution, with controlled accuracy, of IEs met in several hot topics in microwaves and photonics. The corresponding quadrature formulas have been derived earlier; however, they are applied here to new types of IEs, both regular and singular, on finite interval and on semi-axis, with and without a singularity at the endpoints and so on.

The remainder of the paper is structured as follows. Section 2 is devoted to the search for the natural modes of a 2-D microcavity laser, that is, a dielectric open resonator filled with a gain material. This problem is cast to two coupled FIE-2 on a closed contour with regular and log-singular kernel functions and further reduced to finding the roots of corresponding determinantal equation. Section 3 considers the 2-D scattering of an H-polarized plane wave by flat silver strips in the optical range. Using the generalized boundary conditions (GBC), it is reduced to the pair of decoupled IEs on the strip median lines, one log-singular and another hyper-singular, for the magnetic and electric currents, respectively. Two different discretization schemes are applied: one based on the Gauss–Legendre quadratures and another on the weighted Chebyshev quadratures. Section 4 deals with the 3-D problem of an electric dipole radiating in the presence of a thin dielectric disk. GBC are introduced at the disk median section, and the problem is split to finding independent Fourier components. Then the vector Hankel transform helps reduce the problem, for each azimuthal component, to a set of two decoupled dual IEs in transform domain, and MAR is applied to convert them to FIE-2 with integration along a semi-axis. Here discrete model is built using several Gauss quadratures adapted to the integrand behavior on different parts of semi-axis. In Section 5, the 3-D scattering by an arbitrary finite zero-thickness PEC reflector is considered. After splitting the problem to independent Fourier components in azimuth, each of them is reduced to two coupled hyper-singular IEs on the reflector cross-section for the components of induced electric current. Discretization of the latter equations involves new quadrature formulas for the singular and regular integrals that take into account the behavior of the unknown functions at the rim of reflector via Chebyshev weights. Some of the conclusions are summarized in Section 6.

Throughout the paper, the time dependence $e^{-i\omega t}$ is implied and omitted.

2. LOGARITHMIC-SINGULAR IEs ON A CLOSED CONTOUR: NATURAL MODES OF A 2-D MICROCAVITY LASER

In this section, we consider a 2-D electromagnetic model of an active dielectric microcavity or a 2-D laser (Figure 1). We will neglect all non-electromagnetic mechanisms and effects that are relevant to lasing and work only with Maxwell equations. Our aim is to determine the frequencies and threshold values of material gain of the lasing modes, together with their fields in the near and far zones. This implies consideration of an eigenvalue problem (no incident field is present). Although this can be performed using both volume and boundary IEs, the latter ones are potentially more economic because of necessity of discretization of the contour of cavity instead of its inner area. Still it is known that

DOI: 10.1002/jnm

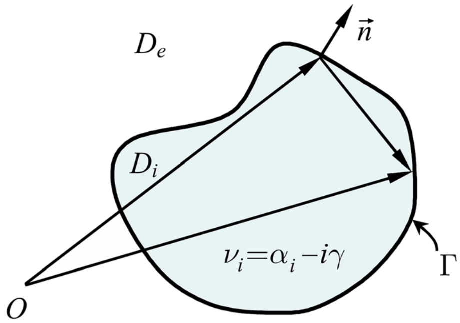

Figure 1. Two-dimensional dielectric resonator of arbitrary shape.

many forms of boundary IEs possess spurious eigenvalues (also known as false resonances), which are inherited by the discrete versions of these IEs and spoil the performance of associated numerical techniques [2]. Fortunately, there exists a set of boundary IEs free of these demerits: this is so-called Muller IEs, which are FIE-2 because their kernels are either smooth or integrable. It should be noted that we cannot confirm the cited in [3] observation that Muller IEs are 'unstable'; we have failed to find the roots of this observation. In contrast, the paper [11] reported remarkably stable performance of the trigonometric Galerkin projection algorithm based on the Muller IEs in the scattering of waves by dielectric cylinders of arbitrary smooth cross-section.

Denote the interior domain of microcavity as D_i, its closed contour as Γ, and the outer domain as D_e (Figure 1). Consider a function $U(x, y)$, which is either the E_z or the H_z field component. When simulating a microlaser, we are interested in real-valued pairs of numbers (k, γ) generating non-zero functions U solving off Γ, the Helmholtz equation $(\Delta + k^2 v^2)U = 0$ with a piecewise-constant effective refractive index v equal to $v_i = \alpha_i - i\gamma(\gamma > 0)$ in D_i, and $v_e = \alpha_e$ in D_e. Here, the following two-side boundary conditions are required on Γ: $U^e = U^i$ and $\eta_e \partial U^e / \partial n = \eta_i \partial U^i / \partial n$, where the superscripts i and e refer to the corresponding domains, $\eta_{i,e} = 1$ (E-polarization) or $\eta_{i,e} = 1/v_{i,e}^2$ (H-polarization), and $\overrightarrow{n}$ is the outward normal vector to Γ. Furthermore, the time-averaged electromagnetic energy must be locally integrable to prevent source-like field singularities, and the Sommerfeld radiation condition must be satisfied at infinity. This is the lasing eigenvalue problem formulated in [12–14]. Here, frequencies k and threshold gains γ are eigenparameters and form a discrete set on the plane (k, γ).

Introduce the Green's functions $G_j(R) = (i/4)H_0^{(1)}(kv_j R)$ of the corresponding homogeneous media, where $j = i, e, R = \left|\overrightarrow{r} - \overrightarrow{r}'\right|$ is the distance between the points $\overrightarrow{r}$ and $\overrightarrow{r}'$, and $H_0^{(1)}(\cdot)$ is the Hankel function. After applying the second Green's formula to the functions $G_j\left(\overrightarrow{r}, \overrightarrow{r}'\right)$ and U_j, using boundary conditions, and taking into account the properties of single-layer and double layer potentials, we obtain Muller IEs [15] as

$$\varphi\left(\overrightarrow{r}\right) + \int_\Gamma \varphi\left(\overrightarrow{r}'\right) A\left(\overrightarrow{r}, \overrightarrow{r}'\right) \mathrm{d}l' - \int_\Gamma \psi\left(\overrightarrow{r}'\right) B\left(\overrightarrow{r}, \overrightarrow{r}'\right) \mathrm{d}l' = 0, \tag{1}$$

$$\frac{\eta_i + \eta_e}{2\eta_e} \psi\left(\overrightarrow{r}\right) + \int_\Gamma \varphi\left(\overrightarrow{r}'\right) C\left(\overrightarrow{r}, \overrightarrow{r}'\right) \mathrm{d}l' - \int_\Gamma \psi\left(\overrightarrow{r}'\right) D\left(\overrightarrow{r}, \overrightarrow{r}'\right) \mathrm{d}l' = 0, \tag{2}$$

where $\mathrm{d}l'$ is the element of the arc on Γ, $\varphi\left(\overrightarrow{r}\right) = U_i\left(\overrightarrow{r}\right)$ and $\psi\left(\overrightarrow{r}\right) = \partial U_i\left(\overrightarrow{r}\right)/\partial n, \quad \rightarrow r \in \Gamma$.

Here, the kernel functions are

$$A\left(\overrightarrow{r}, \overrightarrow{r}'\right) = \partial G_i\left(\overrightarrow{r}, \overrightarrow{r}'\right)/\partial n' - \partial G_e\left(\overrightarrow{r}, \overrightarrow{r}'\right)/\partial n', \tag{3}$$

$$B\left(\overrightarrow{r}, \overrightarrow{r}'\right) = G_i\left(\overrightarrow{r}, \overrightarrow{r}'\right) - \eta_i/\eta_e G_e\left(\overrightarrow{r}, \overrightarrow{r}'\right), \tag{4}$$

$$C\left(\overrightarrow{r}, \overrightarrow{r}'\right) = \partial^2 G_i\left(\overrightarrow{r}, \overrightarrow{r}'\right)/\partial n \partial n' - \partial^2 G_e\left(\overrightarrow{r}, \overrightarrow{r}'\right)/\partial n \partial n', \tag{5}$$

$$D\left(\overrightarrow{r}, \overrightarrow{r}'\right) = \partial G_i\left(\overrightarrow{r}, \overrightarrow{r}'\right)/\partial n - (\eta_i/\eta_e)\partial G_e\left(\overrightarrow{r}, \overrightarrow{r}'\right)/\partial n \tag{6}$$

DOI: 10.1002/jnm

Note that the kernel functions $A(t,\tau)$ and $D(t,\tau)$ are continuous, and the kernel functions $B(t,\tau)$ and $C(t,\tau)$ have logarithmic singularities.

There are several ways of efficient discretization of the boundary IEs. For instance, this can be performed with the aid of a Galerkin projection method that has been applied to the Muller IEs in [11]. Another efficient technique is the method of quadratures, also known as the Nystrom method [16,17]. This latter method is based on the replacement of the integrals with approximate sums using the appropriate quadrature formulas. We will use these formulas here as well.

We will assume that the contour of integration Γ admits a regular analytical parameterization with the aid of a function $r(t)=\{x(t),y(t)\}, t\in[0,2\pi]$. As some of the kernel functions have logarithmic singularities, it is convenient to represent all of the kernels (1) and (2) in such a way that these singularities are extracted [17]:

$$F(t,\tau) = F_1(t,\tau)\ln\left[4\sin^2((t-\tau)/2)\right] + F_2(t,\tau), \quad F = A, B, C, D, \tag{7}$$

$$A_1(t,\tau) = (-1/4\pi)[k_i J_1(k_i R) - k_e J_1(k_e R)]\left(\overrightarrow{R}\cdot\overrightarrow{n}'\right)/R, \tag{8}$$

$$B_1(t,\tau) = (-1/4\pi)[J_0(k_i R) - (\eta_i/\eta_e)J_0(k_e R)], \tag{9}$$

$$\begin{aligned} C_1(t,\tau) = {} & (1/4\pi)\left[k_i^2 J_2(k_i R) - k_e^2 J_2(k_e R)\right]\left(\overrightarrow{R}\cdot\overrightarrow{n}'\right)\left(\overrightarrow{R}\cdot\overrightarrow{n}\right)/R^2 \\ & -(1/4\pi)[k_i J_1(k_i R) - k_e J_1(k_e R)]\left(\overrightarrow{n}'\cdot\overrightarrow{n}\right)/R, \end{aligned} \tag{10}$$

$$D_1(t,\tau) = (1/4\pi)[k_i J_1(k_i R) - (\eta_i/\eta_e)k_e J_1(k_e R)]\left(\overrightarrow{R}\cdot\overrightarrow{n}\right)/R, \tag{11}$$

and $\left(\overrightarrow{a}\cdot\overrightarrow{b}\right)$ is an inner vector product. The second term on the right hand side of (7) is defined by $F_2 = F - F_1$, $F=A,B,C,D$. Then the integrals are approximated by two different quadrature rules for the regular and singular parts. We use an equidistant set of points $t_p=\pi p/N$, $p=0,1,\ldots,2N-1$ and quadrature rule [16]

$$\int_0^{2\pi} ln\left[4\sin^2((t-\tau)/2)\right]F_1(t,\tau)f(\tau)L(\tau)\mathrm{d}\tau = \sum_{p=0}^{2N-1} P_p^{(N)}(t)F_1\left(t,t_p\right)f\left(t_p\right)L\left(t_p\right) \tag{12}$$

$$P_p^{(N)}(t) = -(2\pi/N)\sum_{m=1}^{N-1}\cos\left[m\left(t-t_p\right)\right]/m - \pi\cos\left[N\left(t-t_p\right)\right]/N^2 \tag{13}$$

and a trapezoidal rule for 2π-periodic functions [18]

$$\int_0^{2\pi} F_2(t,\tau)f(\tau)L(\tau)d\tau = (\pi/N)\sum_{p=0}^{2N-1} F_2\left(t,t_p\right)f\left(t_p\right)L\left(t_p\right) \tag{14}$$

where $L(t) = \sqrt{(\mathrm{d}x/\mathrm{d}t)^2 + (\mathrm{d}y/\mathrm{d}t)^2}$ is the Jacobian and $f=\varphi,\psi$ are unknown functions.

By evaluating the integrals from (1)–(2) for each $t=t_s$ with the aid of (12)–(14), we obtain a determinantal equation for eigenvalues. Then, a secant-type iterative method is used to find the eigenvalues numerically, with circular-cavity eigenvalues taken as initial guess.

Consider a spiral-shaped microcavity as an example. For the boundary representation we use the following smooth function: $\overrightarrow{r}(t) = \{r(t)\cos(t), r(t)\sin(t)\}, t\in[0,2\pi]$ [19], where

$$r(t) = \begin{cases} 1 - \delta/4\pi\left[(2\pi-\beta)/\beta t - \pi/\beta^2 t^2 - \pi\right], & t\in[0,\beta) \\ 1 + \delta/4\pi t, \quad t\in[\beta, 2\pi-\beta] \\ 1 + \delta/4\pi\left[(2\pi-\beta)/\beta(2\pi-t) - \pi/\beta^2(2\pi-t)^2 + \pi\right], & t\in(2\pi-\beta, 2\pi] \end{cases} \tag{15}$$

Here, $\delta=d/a$ is the normalized step depth, a is the spiral radius at $t=0$, and β is the tilt angle from the x-axis. With this parameterization of the spiral contour, we obtain a smooth curve, however its second derivative $r''(t)$ has two finite jumps at $t=\beta$ and $t=2\pi-\beta$. Then the integrand functions $F_{1,2}(t,\tau)f(\tau)L(\tau)\in C[0,2\pi]$. This circumstance limits the rate of convergence of the algorithm. An

DOI: 10.1002/jnm

example of the actual behavior of the computational errors for the eigenvalues in the case of a spiral resonator is shown in Figure 2(a) as a function of N.

Considering the accuracy of computations, we can note that if the integrand function is analytic and 2π periodic, then according to [17], the error associated with (12) and (13) has the order of $Q[\exp(-\sigma N)]$, where $2N$ is the number of nods in the quadrature and σ is the half-width of the strip in the complex plane where the integrand functions $F_{1,2}(t,\tau)f(\tau)L(\tau)$ can be continued holomorphically.

Relaxation of the requirements to the smoothness of the integrand functions leads to smaller rates of convergence of the algorithm. For example, the error of the quadrature formula (12) amounts $Q(C/N^{r+\varepsilon}), C = \text{const}$ under the assumption that that the function factor at the logarithm belongs to the class of Holder-continuous functions, $C^{r,\varepsilon}$ (i.e., r times continuously differentiable, with the r as the derivative satisfying the Holder condition with index $\varepsilon \in (0,1]$) [17]. In (14), the error of approximation for the 2π-periodic functions of the class C^r(i.e., r times continuously differentiable functions) has the order of $Q(N^{-r})$.

A microlaser shaped as a circular disk provides exponentially low thresholds of the whispering-gallery modes, [12,13], however the emission directivity is equal to 2 only. We can consider the spiral contour as an asymmetrically deformed circle, the measure of perturbation being the step height, $d/\lambda = \delta\kappa/2\pi$ (if $d = 0$ the contour turns to circular). In (15), the parameter β is also involved, responsible for the inclination of the step at the contour. Therefore at the discretization, the distance between the adjacent nods should be kept smaller than β. If the mesh of nodes is equidistant, then very small values of β entail very large numbers of nodes and correspondingly large computation time, thus making the algorithm less efficient (although still convergent).

The modes of the spiral microcavity originate from the double degenerate modes $H_{m,n}, m > 0$ of the circular resonator that are split due to the removal of degeneracy caused by the loss of rotational symmetry. The modes in every doublet are standing waves close to each other in frequency but with lower and higher values of thresholds. Therefore, we denote these sister modes as $H^{h,l}_{m,n}$, where two lower integer indices, similar to the circular resonator, characterize (now conditionally) the numbers of field variations in azimuth and in radius, respectively, and the lower index corresponds to the value of the lasing threshold. Near-field and far-field radiation patterns of the modes of the doublet $H_{7,1}$ are shown in Figure 3. They have been determined numerically after finding the corresponding characteristic numbers and characteristic vectors of the homogeneous matrix equation obtained via the explained previously Nystrom-type discretization of Muller IEs.

Another example is the so-called kite-shaped 2-D cavity whose contour Γ is given by the following smooth (i.e., infinitely continuously differentiable) function, where $t \in [0, 2\pi]$:

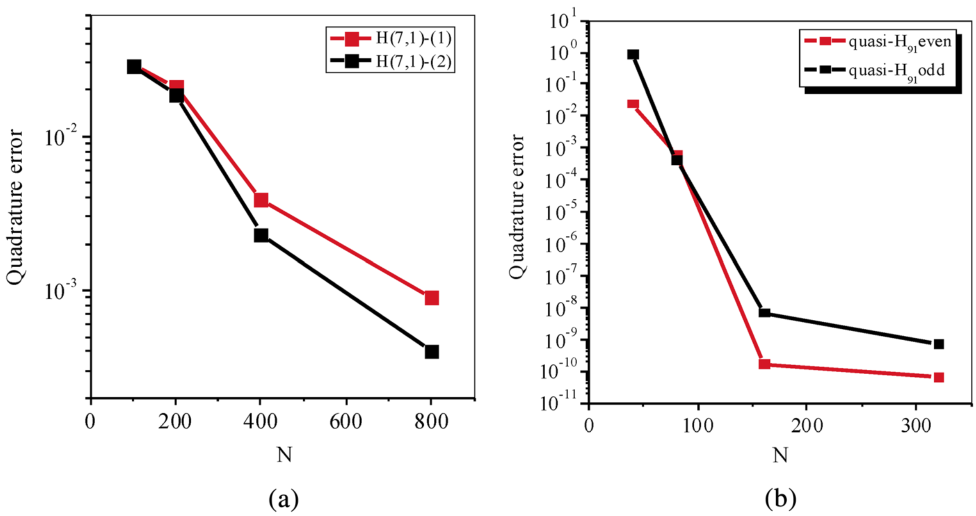

Figure 2. Computational errors associated with the lasing eigenvalues as a function of the order of interpolation scheme (a) for the doublet $H^{h,l}_{7,1}$ in a spiral-shaped cavity $d = 1.0a$, $\beta = \pi/100$ and (b) for the doublet quasi-$H_{\{9,0\}}$ even/odd in a kite cavity, $\delta = 0.5$. Other parameters $\alpha_i = 2.63$, $\alpha_e = 1$.

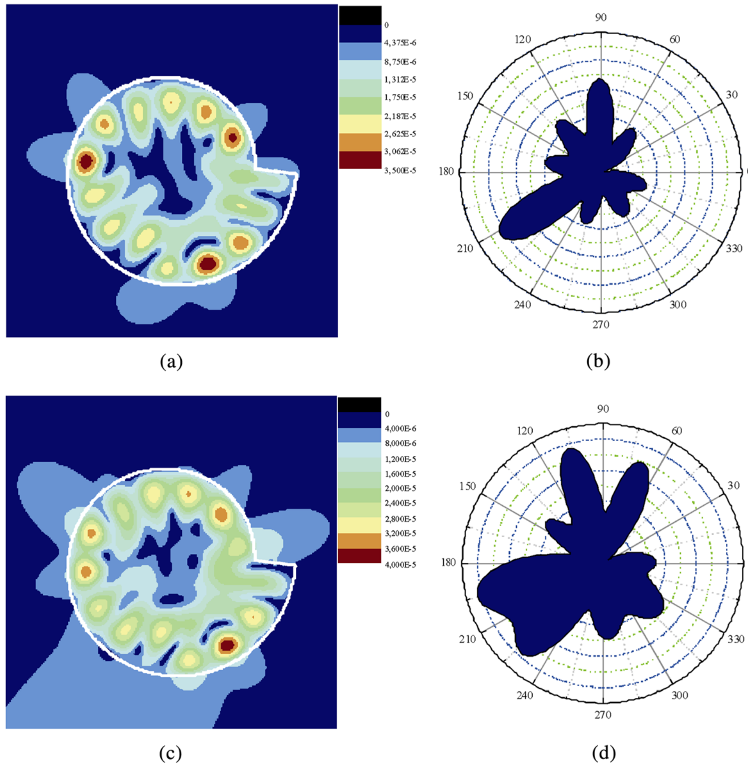

Figure 3. Near and far fields $|H_z|$ for the modes of the doublet $H^{l}_{7,1}$: (a) and (b) $ka=3.2962$, $\gamma=2.52*10^{-2}$; $H^{h}_{7,1}$: (c) and (d) $ka=3.2714$, $\gamma=3.048*10^{-2}$. Other parameters are $d=1.0a$, $\beta=\pi/100$, $\alpha_i=2.63$, $\alpha_e=1$, $N=400$.

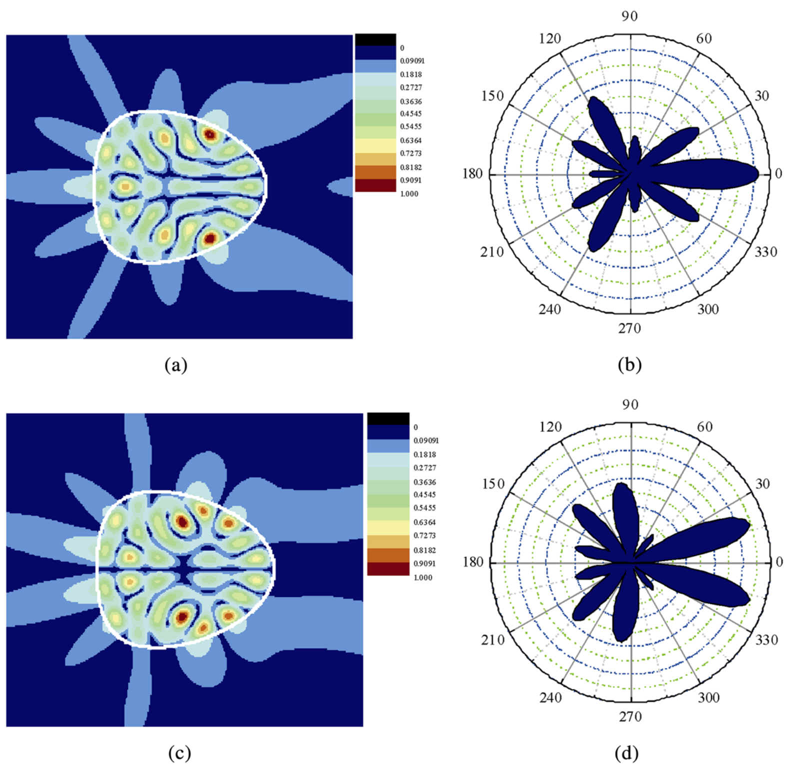

Figure 4. Normalized near-field and far-field emission patterns $|H_z|^2$ for $\delta=0.165$ which corresponds to the maximum of directivity: (a) and (b) $H_{9,1}$ even and (c) and (d) $H_{9,1}$ odd. Other parameters $\alpha=2.63$, and $N=50$.

DOI: 10.1002/jnm

$$\mathrm{r}(t) = \{x(t), y(t)\}, \quad x(t) = a(\cos t + \delta\cos 2t - \delta), \quad y(t) = a\sin t \tag{16}$$

Here, δ is the contour shape deformation parameter, so that if $\delta = 0$ then (16) is a circle of radius a. The shape of the far-field radiation pattern changes very dramatically with the growth of δ. In Figure 4, the field patterns of the modes quasi-$H_{9,1}$ are shown for $\delta = 0.165$. This value of the kite cavity deformation parameter provides the maximum values of directivity for both modes in the studied range of δ variation.

More numerical results related to the analysis of lasing modes of 2-D spiral and kite-shaped active microcavities can be found in the contributed papers [20–22].

3. LOGARITHMIC-SINGULAR AND HYPER-SINGULAR IEs ON A STRAIGHT INTERVAL: 2-D PLASMON-ASSISTED SCATTERING OF LIGHT BY METALLIC NANOSTRIPS

In this section, we consider the 2-D scattering of an H-polarized light of the visible range by a finite periodic coplanar grating of multiple thin noble-metal nanosize strips of the same width d and thickness h in free space (Figure 5), separated by identical gaps g. Note that this specific arrangement is not a limitation for the method presented further. In fact, each strip and gap width may have different values, and even the orientation of strips may be arbitrary.

In principle, such a problem can be studied with a variety of convergent numerical techniques. This can be performed using either a volume IE or a set of boundary IEs. Here, the volume IE implies discretization of the strip's area; besides in the H-case, it is a singular IE and thus needs special treatment. In contrast, the boundary IEs can be non-singular and lead to more economic algorithms as they need discretization only of the strip boundary, which can be characterized using a smooth function. It should be emphasized, however, that the Muller IEs considered in the previous section are the most attractive because they are FIE-2 with smooth and integrable kernels and they have no spurious eigenvalues, which plague other forms of the boundary IEs. As for discretization of these IEs, one can use the Nystrom method for periodic functions presented in Section 2 or trigonometric Galerkin projection method of [11]; both are convergent although the sharpness of smoothed corners and the aspect ratio of the strip will contribute to the matrix size necessary for achieving desired accuracy. In general, it is known that volume IEs lead to matrix equations counting some 10^4 unknowns even for sub-wavelength scatterers and that boundary IEs lead to some 10^2 or larger numbers of unknowns. If the strips are multiple, these values should be multiplied with their number that may result in numerically heavy problem. Therefore, it is reasonable to consider the ways of building more economic numerical models.

When considering the noble metal strips illuminated by the light in the visible range, researchers have the wavelength in the range between 300 and 900 nm, whereas typical width of the strips is from 50 to 1000 nm and their thickness is from 5 to 20 nm. These values of thickness are, firstly, smaller than the skin-depth (20 nm in the visible) and, secondly, some 15 to 180 times smaller than the wavelength, that is, $h << \lambda$.

Keeping this in mind, we can neglect the internal fields inside the strips and instead impose the two-side GBC for the external field limiting values at the strip median lines $L_j = \{(x, y) : x \in [a_j, b_j], y = 0\}$ [23],

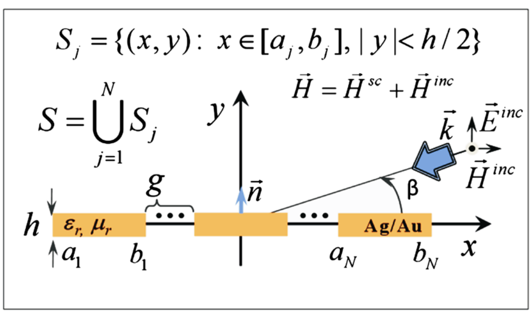

Figure 5. Geometry of a coplanar multi-strip nanostructure illuminated by a plane wave.

$$\partial\left[H_z^+\left(\vec{r}\right)+H_z^-\left(\vec{r}\right)\right]/\partial\vec{n}=-i2kR\left[H_z^+\left(\vec{r}\right)-H_z^-\left(\vec{r}\right)\right],$$
$$\left[H_z^+\left(\vec{r}\right)+H_z^-\left(\vec{r}\right)\right]=i2Qk^{-1}\partial\left[H_z^+\left(\vec{r}\right)-H_z^-\left(\vec{r}\right)\right]/\partial\vec{n} \quad (17)$$

Here, the coefficients

$$R=(i/2)Z\cdot\cot(kh\sqrt{\varepsilon_r}/2), Q=(i/2)Z^{-1}\cdot\cot(kh\sqrt{\varepsilon_r}/2) \quad (18)$$

are the normalized electric and magnetic resistivities, that is, functions of the strip permittivity, thickness and frequency, and $Z=\sqrt{1/\varepsilon_r}$ is the relative impedance of the strip material.

The total magnetic field at $\vec{r}=(x,y)\in R^2$ is a sum of the incident and scattered fields,

$$H_z\left(\vec{r}\right)=e^{-ik(x\cos\beta+y\sin\beta)}+\sum_{j=1}^{N}\left[k\int_{L_j}v_j\left(\vec{r}'\right)G\left(\vec{r},\vec{r}'\right)\mathrm{d}\vec{r}'+\int_{L_j}w_j\left(\vec{r}'\right)\frac{\partial G\left(\vec{r},\vec{r}'\right)}{\partial\vec{n}'}\mathrm{d}\vec{r}'\right], \quad (19)$$

where $k=2\pi/\lambda, G\left(\vec{r},\vec{r}'\right)=(i/4)H_0^{(1)}\left(k\left|\vec{r}-\vec{r}'\right|\right)$ is the Green's function of the 2-D Helmholtz equation, and unknown functions $v_j\left(\vec{r}\right)$ and $w_j\left(\vec{r}\right)(j=1,\ldots,N)$ are electric and magnetic surface currents induced on the strips.

Substituting (19) into (17) and using the properties of the limit values of potentials at the integration contour, we obtain two independent sets of coupled IEs of the second kind. One of them contains IEs with logarithmic-type singularities for all $v_j(x)$, and another contains IEs with hyper-type singularities for all $w_j(x)$:

$$4Qv_s(x_0)+k\sum_{j=1}^{N}\int_{L_j}v_j(x)H_0^{(1)}(k|x-x_0|)\mathrm{d}x=f_v^s(x_0)\equiv 4ie^{-ikx_0\cos\beta}, s=1,\ldots,N \quad (20)$$

$$4Rw_s(x_0)+\sum_{j=1}^{N}\int_{L_j}w_j(x)|x-x_0|^{-1}H_1^{(1)}(k|x-x_0|)\mathrm{d}x=f_w^s(x_0)\equiv 4\sin\beta e^{-ikx_0\cos\beta}, s=1,\ldots,N \quad (21)$$

Note that the integral terms in (21) are understood in the sense of finite part of Hadamard if $x_0\in L_j$. Further, we introduce new unknown functions $\tilde{w}_j(x)=dw_j(x)/\left[\left(b_j-x\right)\left(a_j+x\right)\right]^{1/2}$ and change the variables to $t,t_0:|t|\le 1, |t_0|<1$ according to $x=(d/2)t+j(d+g), x_0=(d/2)t_0+j(d+g)$,

$$4Qv_s(t_0)+\chi_s\int_{-1}^{1}v_s(t)H_0^{(1)}(\kappa|t-t_0|)\mathrm{d}t+\sum_{j=1,j\neq s}^{N}\int_{-1}^{1}v_j(t)K_j^v(\kappa,t,t_0)\mathrm{d}t=f_v^s(t_0), \quad s=1,\ldots,N, \quad (22)$$

$$4R\tilde{w}_s(t_0)+\xi_s\int_{-1}^{1}\tilde{w}_s(t)\sqrt{1-t^2}\frac{H_1^{(1)}(\kappa|t-t_0|)}{|t-t_0|}\mathrm{d}t+\sum_{j=1,j\neq s}^{N}\int_{-1}^{1}\tilde{w}_j(t)\sqrt{1-t^2}K_j^w(\kappa,t,t_0)\mathrm{d}t=f_w^s(t_0), \quad (23)$$

where $\kappa=kd/2, \chi_s$ and $\xi_s(s=1,\ldots,N)$ are known coefficients, and $K_j^w(\kappa,t,t_0), K_j^v(\kappa,t,t_0)$ are known regular functions.

In view of asymptotic expansions for the Hankel functions, the singular kernels functions can be represented as

$$H_0^{(1)}(\kappa|t-t_0|)=(2i/\pi)\ln|t-t_0|+M_v(\kappa,t,t_0), \quad (24)$$

$$H_1^{(1)}(k|t-t_0|)|t-t_0|^{-1}=-(2/\pi\kappa)|t-t_0|^{-2}+(ik/\pi)\ln|t-t_0|+M_w(\kappa,t,t_0). \quad (25)$$

Substituting (24) and (25) into (22) and (23), respectively, we isolate the singularities. For the discretization of the resulted sets of IEs, we use two Nystrom-type methods with different quadrature rules of interpolation type. For IEs (22), we apply the Gauss–Legendre quadrature formulas of the n_v order with the nodes which are nulls of the Legendre polynomials $P_{n_v}\left(\tau_j\right)=0, j=1,\ldots,n_v$. Then, for

DOI: 10.1002/jnm

the singular and regular parts, respectively, we obtain

$$\int_{-1}^{1} v_j(t)\ln|t-t_0|\mathrm{d}t = \sum_{i=1}^{n_v} A_i^{n_v} S(\tau_i, t_0) v_j(\tau_i), \tag{26}$$

$$\int_{-1}^{1} v_j(t) R_v(t,t_0)\mathrm{d}t = \sum_{i=1}^{n_v} A_i^{n_v} v_j(t_i) R(t_i, t_0) \tag{27}$$

where $S(t,t_0) = \ln\left(1-t_0^2\right)/2 + Q_1(t_0) + \sum_{l=1}^{n_v-1} P_l(t)[Q_{l+1}(t_0) - Q_{l-1}(t_0)]$ and $A_i^{n_v} = 2/\left[P_{n_v}{}'(\tau_i)^2\left(1-\tau_i^2\right)\right]$.

For IEs (23), Gauss–Chebyshev quadrature formulas of the n_w order with the weight $\sqrt{1-t^2}$ are more efficient, with Chebyshev nulls of the second type $t_j = \cos(\pi j/(n_w+1)), j = 1, 2, \ldots, n_w$ for discretization nodes. Therefore, for the singular and regular parts we have

$$\int_{-1}^{+1} \frac{\tilde{w}_j(t)}{(t-t_0)^2}\sqrt{1-t^2}\mathrm{d}t = \frac{\pi}{n_w+1}\sum_{j=1, j\neq s}^{n_w} \tilde{w}_j(t_i)\frac{\left(1-t_i^2\right)\left(1-(-1)^{i+s}\right)}{(t_i-t_0)^2} - \frac{\pi(n_w+1)}{2}\tilde{w}_j(t_0), \tag{28}$$

$$\int_{-1}^{+1} \tilde{w}_j(t)\ln|t-t_0|\sqrt{1-t^2}\mathrm{d}t = \frac{\pi}{(n_w+1)}\sum_{i=1}^{n_w} \tilde{w}_j(t_i)\left(t_i^2-1\right)\left[\ln 2 + 2\sum_{k=1}^{n_w}\frac{T_k(t_i)T_k(t_0)}{k} + \frac{(-1)^i}{n_w+1}T_k(t_0)\right], \tag{29}$$

$$\int_{-1}^{+1} \tilde{w}_j(t) R_w(t,t_0)\sqrt{1-t^2}\mathrm{d}t = \frac{\pi}{n_w+1}\sum_{i=1}^{n_w} \tilde{w}_j(t_i) R_w(t_i,t_0)\left(1-t_i^2\right), \quad \forall t_0 \in (-1,1). \tag{30}$$

Here, $R_v(t,t_0), R_w(t,t_0)$ can be arbitrary regular functions on the interval $[-1,1]$, $T_l(t)$ is Chebyshev polynomial of the second kind, and $P_l(t), Q_l(t)$ are Legendre polynomial and Legendre function of the l order, respectively. In the capacity of collocations nodes, we choose corresponding discretization nodes.

As a result, we derive two independent sets of matrix equations of orders n_v and n_w for the values $v_j(\tau_i)$ and $\tilde{w}_j(t_k)$, representing a discrete model of our IEs (20) and (21), respectively. On solving them numerically, we obtain approximate solutions of these IEs in the form of interpolations polynomials for the unknown surface currents.

The presented numerical algorithms of solving (20) and (21) belong to the Nystrom methods [6–10], are efficient and reliable and have theoretically guaranteed convergence (at least as $Q(1/n_v)$ and $Q(1/n_w)$) and controlled accuracy of computations. For the demonstration of the actual rate of convergence, we have computed the root mean square deviations $\varepsilon_{v(w)} = \left|\theta_{v(w)}^{n_v(n_w)}/\theta_{v(w)}^{2n_v(2n_w)} - 1\right|$ of the uniform norms of the surface current functions, $\theta_v = \max_{j=1,\ldots N, k=1,\ldots n_v}\left|v_j(\tau_k)\right|$ and $\theta_w = \left(\sum_{j=1}^{N}\left\|\tilde{w}_j\right\|^2\right)^{1/2}$, where $\left\|\tilde{w}_j\right\|^2 = \int_{-1}^{1}\left|\tilde{w}_j(t)\right|^2\sqrt{1-t^2}\mathrm{d}t$, versus the discretization orders n_v, and n_w, respectively, in Figure 6 (a) and (b).

The errors decrease rapidly confirming the fast rate of convergence and solution stability of the proposed Nystrom method and quadrature rules used. For instance, to achieve four-digit accuracy in the analysis of a 3λ strip-like scatterer one can take $n_v = n_w = 20$. This is by one and three orders of magnitude smaller than with boundary and volume IEs, respectively.

To illustrate the potentialities of the developed method in computational photonics, we have studied the scattering and absorption of light by the grating of $N = 11$ thin coplanar silver nanostrips (Figure 7). As the noble metals display large dispersion in the visible, the dielectric function of silver was taken from the experimental measurements published in [24]. In Figure 7(a) and (b), the plots of the normalized total scattering cross-section and absorption cross-section of the mentioned grating are shown as a function of the wavelength at the inclined incidence.

More numerical results related to the modeling of the wave scattering and absorption by stand-alone thin strips made of conventional dielectrics and noble metals can be found in the contributed papers [25–27].

4. NON-SINGULAR IEs ON A SEMI-AXIS: ENHANCEMENT OF SPONTANEOUS EMISSION IN THE PRESENCE OF A THIN 3-D DIELECTRIC DISK

In this section, we consider the problem of diffraction of a given time-harmonic electromagnetic field by a thinner-than-wavelength high-contrast dielectric disk of radius a (Figure 8, where the axis horizontal electrical dipole is shown as a source of the incident field). In principle, this 3-D problem can be treated using volume or boundary IEs, which can be split into separate IEs of smaller dimensionality for each of the field Fourier components in azimuth. However, all considerations about comparative properties of volume and boundary IEs discussed in the beginning of Section 3 are valid. In view of large size of matrices appearing with 3-D volume and boundary IEs, our aim is to exploit the small thickness of disk and build more economic and still convergent numerical technique.

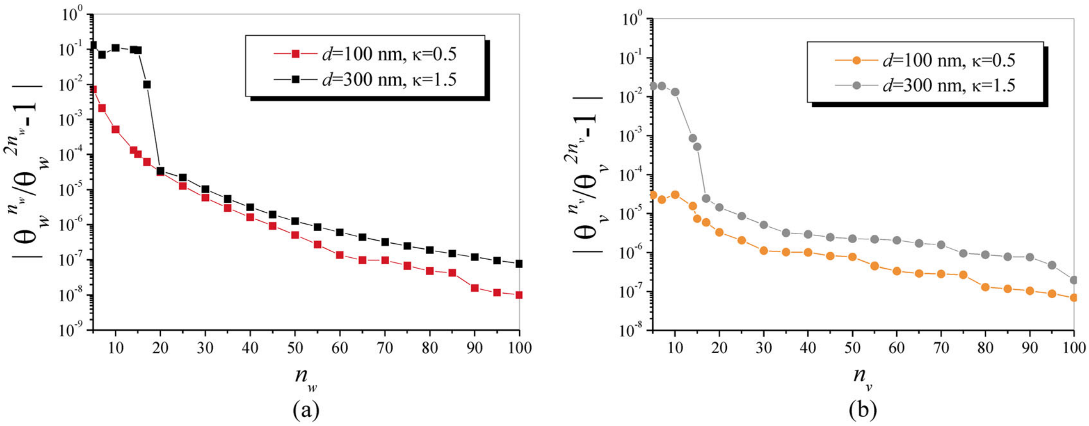

Figure 6. The computation errors (a) ε_v and (b) ε_w as a function of the quadrature orders, n_v and n_w, respectively, for the ensemble of $N=11$ strips with $h=5$ nm, $g=20$ nm for $\kappa=0.5$ and $\kappa=1.5$ under the inclined incidence of H-wave at $\beta=\pi/4$.

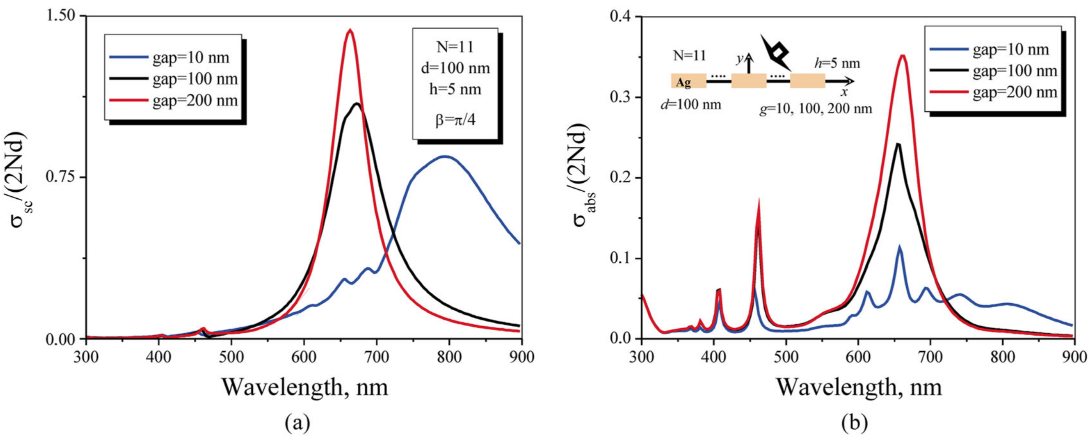

Figure 7. Spectra of the normalized (a) total scattering cross-section and (b) absorption cross-section for $N=11$ coplanar strips of the same widths $d=100$ nm and thickness $h=5$ nm strips for the different gaps values at the inclined ($\beta=\pi/4$) incidence; discretization parameters are $n_v=n_w=20$.

DOI: 10.1002/jnm

Assume that the center of the disk is located at the point ($\rho = 0, z = 0$). Denote the total field as a sum of the incident and scattered fields,

$$E = E_{in} + E_{sc} \quad H = H_{in} + H_{sc}. \tag{31}$$

Introduce ($\rho = r/a, \varphi, \zeta = z/a$) as dimensionless cylindrical coordinates with the origin at the disk center. Demand the incident and scattered fields to satisfy the set of homogeneous Maxwell equations outside of the sources and the disk,

$$\text{curl}\, E = i\, ka\, Z_0 H, \quad Z_0\, \text{curl}\, H = -i\, ka\, E \tag{32}$$

and the generalized boundary conditions of the same type as (17) on the disk surface

$$\left[E_{tg}^{+} + E_{tg}^{-}\right] = 2Z_0 R \cdot \overrightarrow{n} \times \left[H_{tg}^{+} - H_{tg}^{-}\right], Z_0\left[H_{tg}^{+} + H_{tg}^{-}\right] = -2Q \cdot \overrightarrow{n} \times \left[E_{tg}^{+} - E_{tg}^{-}\right]. \tag{33}$$

Here, $Z_0 = \sqrt{\mu_0/\varepsilon_0}$ is the free-space impedance and R and Q are the normalized electric and magnetic resistivities. For a thin dielectric disk, they are given by the expressions (18) of the previous section, where $Z = \sqrt{1/\varepsilon_r}$ is the relative impedance of the disk material and ε_r is the relative permittivity. These expressions are valid under the conditions of $\tau << \lambda_0$ and $|\varepsilon_r| >> 1$, where λ_0 is the wavelength in free space and τ is the disk thickness.

On the rest of the plane ($z = 0$), we demand the components of the field to be continuous. Besides, to provide uniqueness of solution, the scattered field must satisfy the 3-D radiation condition and the edge condition (following from the local integrability of power).

Introduce the normal to the disk incident and scattered field components in terms of the scalar Fourier–Bessel transform

$$\begin{pmatrix} E_z^{(in,sc),\,\text{sgn}\left(\zeta-\xi_{(in,sc)}\right)} \\ Z_0 H_z^{(in,sc),\,\text{sgn}\left(\zeta-\xi_{(in,sc)}\right)} \end{pmatrix} = \sum_{m=-\infty}^{\infty} e^{im\varphi} \int_0^{\infty} e^{i\gamma(\kappa)\left|\zeta-\xi_{(in,sc)}\right|} J_m(\kappa\rho) \begin{pmatrix} \kappa e_{m,z}^{(in,sc),\,\text{sgn}\left(\zeta-\xi_{(in,sc)}\right)}(\kappa) \\ \kappa h_{m,z}^{(in,sc),\,\text{sgn}\left(\zeta-\xi_{(in,sc)}\right)}(\kappa) \end{pmatrix} \mathrm{d}\kappa \tag{34}$$

and tangential to the disk field components in term of the vector Fourier–Bessel transform

$$\begin{pmatrix} E_r^{(in,sc),\,\text{sgn}\left(\zeta-\xi_{(in,sc)}\right)} \\ -iE_\varphi^{(in,sc),\,\text{sgn}\left(\zeta-\xi_{(in,sc)}\right)} \end{pmatrix} = \sum_{m=-\infty}^{\infty} e^{im\varphi} \int_0^{\infty} e^{i\gamma(\kappa)\left|\zeta-\xi_{(in,sc)}\right|} \bar{H}_m(\kappa\rho) \begin{pmatrix} \text{sgn}\left(\zeta-\xi_{(in,sc)}\right) i\gamma(\kappa) e_{m,z}^{(in,sc),\,\text{sgn}\left(\zeta-\xi_{(in,sc)}\right)}(\kappa) \\ -ka\, h_{m,z}^{(in,sc),\,\text{sgn}\left(\zeta-\xi_{(in,sc)}\right)}(\kappa) \end{pmatrix} \mathrm{d}\kappa \tag{35}$$

$$\begin{pmatrix} Z_0 H_r^{(in,sc),\,\text{sgn}(\zeta-\xi)} \\ -iZ_0 H_\varphi^{(in,sc),\,\text{sgn}(\zeta-\xi)} \end{pmatrix} = \sum_{m=-\infty}^{\infty} e^{im\varphi} \int_0^{\infty} e^{i\gamma(\kappa)\left|\zeta-\xi_{(in,sc)}\right|} \bar{H}_m(\kappa\rho) \begin{pmatrix} \text{sgn}\left(\zeta-\xi_{(in,sc)}\right) i\gamma(\kappa) h_{m,z}^{(in,sc),\,\text{sgn}\left(\zeta-\xi_{(in,sc)}\right)}(\kappa) \\ ka\, e_{m,z}^{(in,sc),\,\text{sgn}\left(\zeta-\xi_{(in,sc)}\right)}(\kappa) \end{pmatrix} \mathrm{d}\kappa \tag{36}$$

Here, $\gamma(\kappa) = \sqrt{(ka)^2 - \kappa^2}$ is the complex valued function with the chosen branch $\text{Re}(\gamma(\kappa)) \geq 0$, $\text{Im}(\gamma(\kappa)) \geq 0$,

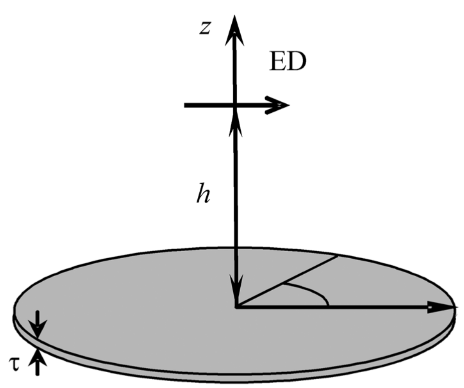

Figure 8. Geometry of elementary electric dipole radiated in the presence of a thin dielectric disk.

DOI: 10.1002/jnm

$$\bar{H}_m(\kappa\rho) = \begin{pmatrix} J'_{|m|}(\kappa\rho) & mJ_{|m|}(\kappa\rho)/(\kappa\rho) \\ mJ_{|m|}(\kappa\rho)/(\kappa\rho) & J'_{|m|}(\kappa\rho) \end{pmatrix} \tag{37}$$

is vector Hankel transform, $e_{m,z}^{(in,sc),\pm}(\kappa)$ and $h_{m,z}^{(in,sc),\pm}(\kappa)$ are images of the normal to the disk field components at over and under the plane ($\zeta = \xi_{in}$) regions for the incident field and at over and under the plane ($\zeta = \xi_{sc} = 0$) for the scattered field, respectively.

Substituting tangential to the disk field components to the generalized boundary conditions, one obtains the following set of coupled dual IEs:

$$\begin{cases} \int\limits_0^\infty \bar{H}_m(\kappa\rho)\begin{pmatrix} \gamma(\kappa)\left(u_m^{sc,-}(\kappa) + u_m^{in,-}(\kappa)\right) + 2R\,ka\,u_m^{sc,-}(\kappa) \\ ika\left(v_m^{sc,+}(\kappa) + v_m^{in,+}(\kappa)\right) + 2R\,i\,\gamma(\kappa)v_m^{sc,+}(\kappa) \end{pmatrix}\mathrm{d}\kappa = \bar{0}\ (\rho < 1) \\ \int\limits_0^\infty \bar{H}_m(\kappa\rho)\begin{pmatrix} ika\,u_m^{sc,-}(\kappa) \\ -\gamma(\kappa)v_m^{sc,+}(\kappa) \end{pmatrix}\mathrm{d}\kappa = \bar{0}\ (\rho > 1) \end{cases} \tag{38}$$

$$\begin{cases} \int\limits_0^\infty \bar{H}_m(\kappa\rho)\begin{pmatrix} \gamma(\kappa)\left(v_m^{sc,-}(\kappa) + v_m^{in,-}(\kappa)\right) + 2Q\,ka\,v_m^{sc,-}(\kappa) \\ -\left(ika\left(u_m^{sc,+}(\kappa) + u_m^{in,+}(\kappa)\right) + 2Q\,i\,\gamma(\kappa)u_m^{sc,+}(\kappa)\right) \end{pmatrix}\mathrm{d}\kappa = \bar{0}\ (\rho < 1) \\ \int\limits_0^\infty \bar{H}_m(\kappa\rho)\begin{pmatrix} ika\,v_m^{sc,-}(\kappa) \\ \gamma(\kappa)u_m^{sc,+}(\kappa) \end{pmatrix}\mathrm{d}\kappa = \bar{0}\ (\rho > 1) \end{cases} \tag{39}$$

where $u_m^{sc,\pm}(\kappa), v_m^{sc,\pm}(\kappa)$ are the images of jumps and average values of the normal to the disk scattered field components: $u_m^{sc,\pm}(\kappa) = \left(e_{m,z}^{sc,+}(\kappa) \pm e_{m,z}^{sc,-}(\kappa)\right)/2$; $v_m^{sc,\pm}(\kappa) = \left(h_{m,z}^{sc,+}(\kappa) \pm h_{m,z}^{sc,-}(\kappa)\right)/2$ (these are four unknown functions of the set of coupled dual IEs) and $u_m^{in,\pm}(\kappa), v_m^{in,\pm}(\kappa)$ are given by the incident field functions. Note that direct numerical solution of these IEs is questionable due to the unpredictable convergence and ill conditioning. Nevertheless, a way to reduce these dual IEs to a set of FIE-2 called the method of analytical regularization [5]. It is based on the inversion of the most singular parts of integral operators of the coupled dual IEs (38) and (39).

Consider the disk excitation by a horizontal elementary electrical dipole located at the axis of the disk on distance h above the disk (Figure 8). In this case, only two azimuthal index values $m = \pm 1$ should be considered, and following the scheme presented in [28], we reduce IEs (38) to the following FIE-2 for the first pair of unknowns $u_{\pm 1}^{sc,-}(\lambda)$ and $v_{\pm 1}^{sc,+}(\lambda)$:

$$u_{\pm 1}^{sc,-}(\lambda) = i\int\limits_0^\infty \kappa^{-1}\left((w(\kappa) + 2Rka)u_{\pm 1}^{sc,-}(\kappa) + \gamma(\kappa)u_{\pm 1}^{in,-}(\kappa)\right)S_{1/2}(\kappa,\lambda)\mathrm{d}\kappa - iA_{\pm 1}^l\frac{2\sqrt{2}}{\sqrt{\pi}}\frac{J_{3/2}(\lambda)}{\lambda^{1/2}} \tag{40}$$

$$\gamma(\lambda)v_{\pm 1}^{sc,+}(\lambda) = -\frac{ka}{2R}\lambda^{1/2}\int\limits_0^\infty \kappa^{-1/2}\left(v_{\pm 1}^{sc,+}(\kappa) + v_{\pm 1}^{in,+}(\kappa)\right)S_2(\kappa,\lambda)\mathrm{d}\kappa \mp 2D_{\pm 1}^r J_1(\lambda) \tag{41}$$

$$\frac{4}{3}A_{\pm 1}^l - (ka)^{-1}D_{\pm 1}^r = \sqrt{\frac{2}{\pi}}\int\limits_0^\infty \kappa^{-3/2}\left((w(\kappa) + 2Rka)u_{\pm 1}^{sc,-}(\kappa) + \gamma(\kappa)u_{\pm 1}^{in,-}(\kappa)\right)J_{3/2}(\kappa)\mathrm{d}\kappa \tag{42}$$

$$\frac{i}{2R}A_{\pm 1}^l + D_{\pm 1}^r = \pm\frac{ka}{2R}\int\limits_0^\infty \kappa^{-1}\left(v_{\pm 1}^{sc,+}(\kappa) + v_{\pm 1}^{in,+}(\kappa)\right)J_1(\kappa)\mathrm{d}\kappa \tag{43}$$

Here $A_{\pm 1}^l$ and $D_{\pm 1}^r$ are unknown constants of integration (to be found),

DOI: 10.1002/jnm

$$S_\mu(\kappa,\lambda)=\kappa^{1/2}\lambda^{1/2}\int_0^1 J_\mu(\kappa v)J_\mu(\lambda v)v\mathrm{d}v=\frac{\kappa^{1/2}\lambda^{1/2}}{\kappa^2-\lambda^2}\left(\lambda J_{\mu-1}(\lambda)J_\mu(\kappa)-\kappa J_{\mu-1}(\kappa)J_\mu(\lambda)\right) \tag{44}$$

and J_v is the Bessel function of v order. One can find a similar FIE-2 for the second pair by substitution of Q to (40)–(43) instead of R and $v_{\pm 1}^{*,-}(\lambda), -u_{\pm 1}^{*,+}(\lambda)$ instead of $u_{\pm 1}^{*,-}(\lambda), v_{\pm 1}^{*,+}(\lambda)$, respectively.

Favorable features of FIE-2 guarantee the uniqueness and existence of their solutions [1,4] and convergence of any numerical algorithm based on a reasonable discretization scheme. In our case we do the following:

(i) Rewrite the set of FIE-2 (40)–(43) in terms of unknown function: $x_{\pm 1}^E(\lambda)=\lambda^{-1}u_{\pm 1}^{sc,-}(\lambda)$, $y_{\pm 1}^E(\lambda)=\gamma(\lambda)\lambda^{-1}v_{\pm 1}^{sc,+}(\lambda), x_m^H(\lambda)=\lambda^{-1}v_{\pm 1}^{sc,-}(\lambda)$ and $y_m^H(\lambda)=-\gamma(\lambda)\lambda^{-1}u_{\pm 1}^{sc,+}(\lambda)$.

(ii) Introduce the truncation number $N\geq ka+1$and truncate the interval of integration to $(0,N)$ for each integral operator of obtained FIE-2.

(iii) Split the interval of integration into four subintervals: $L_1=(0,2/3\cdot ka), L_2=(2/3\cdot ka, ka)$, $L_3=$ $(ka, ka+2/3(N-ka))$ and $L_4=(ka+2/3(N-ka),N)$, and discretize FIE-2 by applying the Nystrom method with the following Gauss-type higher-order quadratures [18]:

$$\int_a^b f(y)\mathrm{d}y=\frac{b-a}{2}\sum_{i=1}^{Q} w_i f\left(y_i^{(1)}\right) \tag{45}$$

$$\int_a^b \frac{f(y)}{\sqrt{b-y}}\mathrm{d}y=2\sqrt{b-a}\sum_{i=1}^{Q/2} w_{Q/2+i} f\left(y_{Q/2+i}^{(2)}\right) \tag{46}$$

$$\int_a^b \frac{f(y)}{\sqrt{a-y}}\mathrm{d}y=-2i\sqrt{b-a}\sum_{i=1}^{Q/2} w_{Q/2+i} f\left(y_{Q/2+i}^{(3)}\right) \tag{47}$$

where $y_i^{(1)}=(b-a)x_i/2+(b+a)/2, y_i^{(2)}=(b-a)\left(1-x_i^2\right)+a, y_i^{(3)}=(b-a)\left(x_i^2-1\right)+$ b, x_i is the ith root of Legendre polynomial $P_Q(x)$ and w_i is correspondent to its quadrature-wise coefficient given by $w_i=2\cdot\left(1-x_i^2\right)^{-1}\left(P'_Q(x_i)\right)^{-2}$.

(iv) Find the unknowns at the grid points by inverting the matrix analog of FIE-2.

(v) Obtain the unknown functions on the $(0,\infty)$ interval by substituting the set of the found values into the discrete analog of FIE-2.

As an illustration of this approach, in Figure 9 we show the dependences of the normalized total radiated power (the same as normalized spontaneous emission rate) of the on-axis horizontal electrical dipole in the presence of a thin dielectric microdisk with thickness $\tau=0.0032a$ and permittivity $\varepsilon_r=25(1+i\delta)$, where $\delta=10^{-2}, 10^{-5}$ correspond to different losses in the disk material. The chosen value of dielectric constant corresponds to HfO_2 in the visible range. Total radiated power is normalized by the free-space radiated power, which is $P_0=(12\pi)^{-1}Z_0\cdot I^2(kd)^2$ where I is the current in the dipole and $d<<\lambda$ is the dipole length. One can see the resonance nature of the radiated power at certain frequencies where the peak values of P_{rad} are several times higher than P_0. They correspond to the radial resonances inside the disk. In Figure 10, we show the normalized radiation patterns, as a function of the elevation angle, for the Poynting vector of the horizontal electrical dipole located above a thin dielectric microdisk with $\varepsilon_r=25(1+i10^{-5})$, in the first three resonances of Figure 9. They demonstrate that at the in-resonance the radiation patterns are dominated by the scattering in the disk plane. This is due to the nature of resonances as standing cylindrical surface waves formed by the principal guided transverse magnetic wave of the dielectric slab excited by the electrical dipole and back-reflected from the disk rim. This supports the validity of empirical approximate model of a 3-D thin disk as a 2-D circle filled with dielectric having bulk refractive index replaced with its effective value [11,12].

DOI: 10.1002/jnm

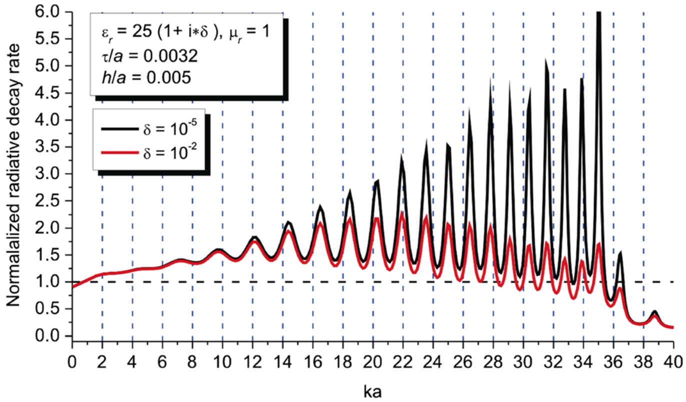

Figure 9. Normalized radiative decay rate versus the dimensionless frequency parameter ka.

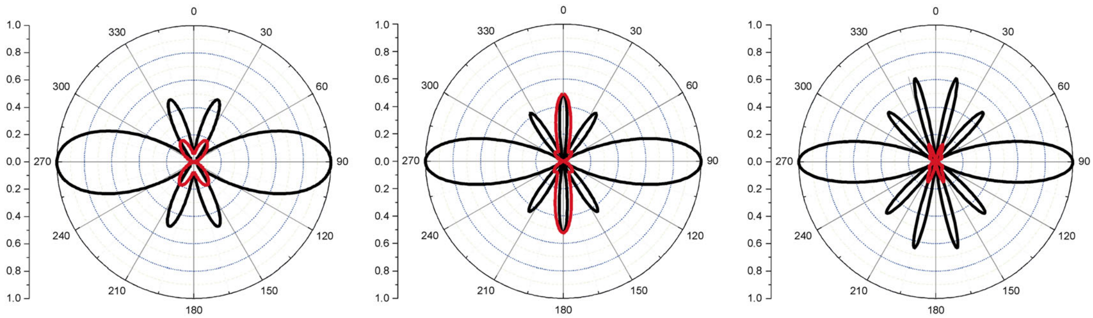

(a) (b) (c)

Figure 10. Normalized radiation patterns for the disk with $\varepsilon_r = 25(1 + i10 - 5)$ in the resonances at (a) $ka = 9.62$, (b) $ka = 13.21$ and (c) $ka = 14.35$ in two planes: $\varphi = 0$ (red) and $\varphi = \pi/2$ (black).

More numerical results related to the spontaneous emission modification due to the presence of disk and also to the beam wave diffraction by the disk can be found in the contributed papers [29] and [30], respectively.

5. SINGULAR AND HYPER-SINGULAR IEs ON A SMOOTH OPEN CONTOUR: 3-D SCATTERING BY A ROTATIONALLY SYMMETRIC ZERO-THICKNESS PEC REFLECTOR

Consider the problem of diffraction of an arbitrary time-harmonic wave $(\vec{E}^{0}, \vec{H}^{0})$ by a zero-thickness PEC open surface of rotation S located in free space (Figure 11). Such surfaces serve as models of thin metallic reflectors for microwave antennas and radar targets. Their analysis methods have been developed in [31,32]; however, convergence of the methods of [33,32] has not been proved mathematically and is questionable, whereas the MAR-based method of [31] is good only for a spherical PEC disk illuminated by a normally incident plane wave.

Denote the total electromagnetic field as $\left(\vec{E}^{tot}, \vec{H}^{tot}\right)$, which is the sum of the incident field $\left(\vec{E}^{0}, \vec{H}^{0}\right)$ and the scattered field $\left(\vec{E}, \vec{H}\right)$. To provide uniqueness of solution, we demand the total field to satisfy the set of homogeneous Maxwell equations outside of S, PEC boundary condition on S, Meixner edge condition at the rim of S and the 3-D radiation condition at infinity.

We choose the cylindrical coordinates ρ, φ, z and introduce the curvilinear orthogonal coordinates q, τ, φ associated with the rotation surface, so that S is created by the rotation of contour C around the z-axis,

$$S : q = q_0, \tau \in [-1, 1], \varphi \in [0, 2\pi]. \tag{48}$$

Then the cylindrical coordinates of a point on S can be found in terms of the curvilinear coordinates as $\rho = \rho(t) = \rho(q_0, t), \varphi, z = z(t) = z(q_0, t)$. We also introduce the Lame coefficients of the coordinates q, τ, φ,

DOI: 10.1002/jnm

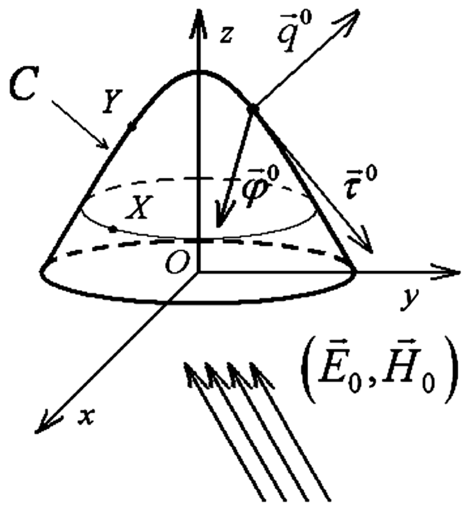

Figure 11. Generic geometry of a finite perfectly electrically conducting surface of rotation.

$$l_q = \sqrt{\left(\rho_q'\right)^2 + \left(z'_q\right)^2}, l_\tau = \sqrt{\left(\rho'_\tau\right)^2 + \left(z'_\tau\right)^2}, l_\phi = \rho, \tag{49}$$

and the unit vectors of curvilinear coordinates,

$$\vec{q}^{\,0} = \left(\vec{x}^{\,0}\rho_q' \cos\varphi + \vec{y}^{\,0}\rho_q' \sin\varphi + \vec{z}^{\,0} z'_q\right)/l_q, \tag{50}$$

$$\vec{\tau}^{\,0} = \left(\vec{x}^{\,0}\rho_\tau' \cos\varphi + \vec{y}^{\,0}\rho_\tau' \sin\varphi + \vec{z}^{\,0} z'_\tau\right)/l_\tau, \tag{51}$$

$$\vec{\varphi}^{\,0} = -\vec{x}^{\,0} \sin\varphi + \vec{y}^{\,0} \cos\varphi. \tag{52}$$

We will use the following notations: $\rho_0 = \rho_0(t), z_0 = z_0(t)$ with $h_\tau = l_\tau(q_0, t), t \in [-1, 1]$ in the case of t being the integration variable, and $\rho = \rho(\tau), z = z(\tau), \tau \in [-1, 1]$ for the observation one.

It is known that the electric field can be expressed in terms of the scalar and vector electromagnetic potentials as

$$\overrightarrow{E} = -\,\mathrm{grad}\Psi - i\omega\overrightarrow{A}, \tag{53}$$

where the vector and scalar potentials can be presented as a convolution of the surface current function with the scalar Green's function and via divergence operation, respectively,

$$\overrightarrow{A}(Y) = (\mu/4\pi)\int_S \overrightarrow{j}(X)e^{-ikL_{XY}}(L_{XY})^{-1}\mathrm{d}S_X, \Psi = (i/\omega\varepsilon_0\mu_0)\,\mathrm{div}\overrightarrow{A} \tag{54}$$

where L_{XY} is the distance from Y to the integration point X.

Then the PEC boundary conditions in the term of potentials are as follows:

$$\lim_{X\to Y}\left[i\omega A_{\tau,\varphi}(X) + \left(1/l_{\tau,\varphi}\right)\Psi'_{\tau,\varphi}(X)\right] = E^0_{\tau,\varphi}(Y), Y \in S, \tag{55}$$

The components of the current density can be presented as a Fourier series in azimuth,

$$j_v(t,\psi) = \sum\nolimits_{M=-\infty}^{\infty} j_v^M(t)e^{iM\psi}, v = \tau, \varphi, \tag{56}$$

and similar series can be written for the incident field on the surface S and the scalar and vector potentials, with coefficients $E_v^{0(M)}(t), A_v^M(q,\tau)$ and $\Psi^M(q,\tau)$, respectively. As shown in [34], the Fourier coefficients of the scalar and vector potentials are expressed through the surface-current coefficients in the following form:

$$A_\tau^M(q,\tau) = \mu/(4\pi l_\tau)\int_{-1}^{1}\left[j_\tau^M(t)\rho_0\left(z'z'_0 S_M + \rho'\rho'_0 S_M^+\right) - j_\varphi^M(t)\rho_0 h_\tau \rho' S_M^-\right]\mathrm{d}t, \tag{57}$$

$$A_\varphi^M(q,\tau) = (\mu/4\pi)\int_{-1}^{1}\left[j_\tau^M(t)\rho_0\rho'_0 S_M^- + j_\varphi^M(t)\rho_0 h_\tau S_M^+\right]\mathrm{d}t, \tag{58}$$

$$\Psi^M(q,\tau) = (-i/4\pi k)Z_0\int_{-1}^{1}\left[j_\tau^M(t)\rho_0\frac{\partial S_M}{\partial t} - iMj_\phi^M(t)h_\tau S_M\right]\mathrm{d}t, \tag{59}$$

$$S_M(q,\tau,t) = S_M = \int_{-1}^{1}\cos(M\psi)\left(e^{-ikL}/L\right)\mathrm{d}\psi \tag{60}$$

$$S_M^+ = (S_{M+1} + S_{M-1})/2, S_M^- = (S_{M+1} - S_{M-1})/2i \tag{61}$$

$$L = \sqrt{\rho^2 + {\rho_0}^2 - 2\rho\rho_0\cos\psi + (z-z_0)^2} \tag{62}$$

Introduce new unknown smooth functions $u^M(t)$ and $w^M(t)$ in conformity with the edge condition as

$$j_\tau^M(t)\rho(t) = u^M(t)\sqrt{1-t^2}, j_\varphi^M(t)h_\tau(t) = w^M(t)/\sqrt{1-t^2} \tag{63}$$

Thus in (55), $\lim\limits_{X\to Y}$ equals to $\lim\limits_{q\to q_0}$ because the point belongs to the surface S if $q=q_0$. If we substitute expressions for $j_v(t,\psi), E_v^{0(M)}(t), A_v^M(q,\tau)$ and $\Psi^M(q,\tau)$ into (55), we obtain a set of equations with 1-D integrals with the function $S_M(q,\tau,t)$ and its first and second derivatives in the kernels. As $S_M(q_0,\tau,t)\underset{t\to\tau}{\cong}(-2/\rho)\ln|\tau-t|$ [34], one cannot move the limit to the integrands of (55) because of non-integrable singularities $Q\left[(\tau-t)^{-2}\right]$.

Introduce the following integral operators [7]:

- hyper-singular integral operator understood in the sense of Hadamard finite part

$$(Au)(\tau) = (1/\pi)\int_{-1}^{1}u(t)\sqrt{1-t^2}/(\tau-t)^2\mathrm{d}t \tag{64}$$

- singular integral operators understood in Cauchy principal value sense with different weights

$$(\Gamma u)(\tau) = (1/\pi)\int_{-1}^{1}u(t)/\left[\sqrt{1-t^2}\cdot(\tau-t)\right]\mathrm{d}t, \tag{65}$$

$$\left(\Gamma^{-1}u\right)(\tau) = (1/\pi)\int_{-1}^{1}u(t)\sqrt{1-t^2}/(\tau-t)\mathrm{d}t, \tag{66}$$

- integral operators with logarithmic kernels

$$\left(L^I u\right)(\tau) = (1/\pi)\int_{-1}^{1}\ln|\tau-t|u(t)\sqrt{1-t^2}\mathrm{d}t, \tag{67}$$

$$\left(L^{II} u\right)(\tau) = (1/\pi)\int_{-1}^{1}\ln|\tau-t|u(t)/\sqrt{1-t^2}\mathrm{d}t, \tag{68}$$

- and integral operators with smooth kernels and weights

$$\left(K^{I,II} u\right)(\tau) = (1/\pi)\int_{-1}^{1}K^{I,II}(\tau,t)u(t)\sqrt{1-t^2}\mathrm{d}t \tag{69}$$

$$\left(K^{II} u\right)(\tau) = (1/\pi)\int_{-1}^{1}K(\tau,t)u(t)/\sqrt{1-t^2}\mathrm{d}t. \tag{70}$$

DOI: 10.1002/jnm

If we take a limit in (56) using the expressions for the vector and scalar potentials (57)–(59), then we obtain a set of two coupled hyper-singular and singular IEs,

$$\begin{pmatrix} a_{11}A + b_{11}\Gamma^{-1} + c_{11}^M L^I + K_{11}^{M(I)} & b_{12}^M\Gamma + c_{12}^M L^{II} + K_{12}^{M(II)} \\ b_{21}^M\Gamma^{-1} + c_{21}^M L^I + K_{21}^{M(I)} & c_{22}^M L^{II} + K_{22}^{M(II)} \end{pmatrix} \cdot \begin{pmatrix} w^M(\tau) \\ u^M(\tau) \end{pmatrix} = \begin{pmatrix} 4ik\rho^3 E_\tau^{0(M)}(\tau)h_\tau(\tau)/Z \\ 4ik\rho^3 E_\varphi^{0(M)}(\tau)/Z \end{pmatrix}, \tag{71}$$

where $M = 0, \pm 1, \pm 2, \ldots$, and the varying coefficients are

$$a_{11}(\tau) = -2\rho^2, b_{11}(\tau) = -\rho^{'}\rho, \tag{72}$$

$$c_{11}^M(\tau) = \left(k^2\rho^2 + M^2\right)\left(\rho^{'2} + z^{'2}\right) - \left(z^{'2} + 3\rho^{'2}\right)/4, \tag{73}$$

$$b_{12}^M(\tau) = 2iM\rho^2, c_{12}^M(\tau) = -iM\rho^{'}\rho, b_{21}^M(\tau) = 2iM\rho, \tag{74}$$

$$c_{21}^M(\tau) = iM\rho^{'}, c_{22}^M(\tau) = -2M^2\rho + 2k^2\rho^3, \tag{75}$$

whereas the smooth kernels are

$$K_{11}^M(\tau,t) = \rho^3\left[\partial^2 S_M/\partial t\partial\tau - k^2\left(\rho^{'}{}_0\rho^{'}S_M^+ + z^{'}{}_0 z^{'} S_M\right)\right] - a_{11}(\tau)/(\tau-t)^2 - b_{11}(\tau)/(\tau-t) - c_{11}^M(\tau)\ln|\tau - t| \tag{76}$$

$$K_{12}^M(\tau,t) = \rho^3\left[k^2\rho_0\rho^{'}S_M^- - iM\cdot\partial S_M/\partial\tau\right] - b_{12}^M(\tau)/(\tau-t) - c_{12}^M(\tau)\ln|\tau-t| \tag{77}$$

$$K_{21}^M(\tau,t) = \rho^3\left[(iM/\rho)\partial S_M/\partial t - k^2\rho^{'}{}_0 S_M^-\right] - b_{21}^M(\tau)/(\tau-t) - c_{21}^M(\tau)\ln|\tau-t| \tag{78}$$

$$K_{22}^M(\tau,t) = \rho^3\left[\left(M^2/\rho\right)S_M - k^2\rho_0 S_M^+\right] - c_{22}^M(\tau)\ln|\tau-t| \tag{79}$$

We use the following interpolation type quadrature formulas [7] for discretization of hyper-singular and singular IEs (71):

- quadrature formulas for a hyper-singular integral,

$$Au_{n-2}\left(t_{0l}^n\right) = \sum\nolimits_{k=0}^{n-2} A_{l,k}u_{n-2}\left(t_{0k}^n\right),\ A_{kk} = -n/2,\ A_{l,k} = \left(1-(-1)^{l+k}\right)\left(1-\left(t_{0k}^n\right)^2\right)\Big/\left[n\left(t_{0l}^n - t_{0k}^n\right)^2\right], l \neq k \tag{80}$$

- quadrature formulas for singular integrals,

$$\begin{gathered} \Gamma^{-1}u_{n-2}\left(t_{0l}^n\right) = \sum\nolimits_{k=0}^{n-2}\Gamma_{l,k}^{-1(I)}u_{n-2}\left(t_{0k}^n\right), \Gamma_{k,k}^{-1(I)} = 0, \\ \Gamma_{l,k}^{-1(I)} = \left(1-(-1)^{l+k}\right)\left(1-\left(t_{0k}^n\right)^2\right)\Big/\left[n\left(t_{0l}^n - t_{0k}^n\right)\right], l \neq k \end{gathered} \tag{81}$$

$$\Gamma^{-1}u_{n-2}\left(t_l^n\right) = \sum\nolimits_{k=0}^{n-2}\Gamma_{l,k}^{-1(II)}u_{n-2}\left(t_{0k}^n\right), \Gamma_{l,k}^{-1(II)} = \left(1-\left(t_{0k}^n\right)^2\right)\Big/\left(\left(t_l^n - t_{0k}^n\right)\cdot n\right) \tag{82}$$

$$\Gamma u_{n-2}\left(t_{0l}^n\right) = \sum_{k=0}^{n-1}\Gamma_{l,k}u_{n-2}\left(t_k^n\right), \Gamma_{l,k} = 1\Big/\left(\left(t_{0l}^n - t_k^n\right)\cdot n\right) \tag{83}$$

- quadrature formulas for integrals with logarithm kernels,

$$L^I u_{n-2}(\tau) = \sum\nolimits_{m=0}^{n-2} L_k^I(\tau)u_{n-2}\left(t_{0k}^n\right) \tag{84}$$

$$L_k^I(\tau) = -\left(1-\left(t_{0k}^n\right)^2\right)\left[\ln 2 + 2\sum\nolimits_{p=1}^{n-1}T_p\left(t_{0k}^n\right)T_p(\tau)/p + (-1)^j T_n(\tau)/n\right]/n \tag{85}$$

DOI: 10.1002/jnm

$$L^{II}u_{n-2}(\tau)=\sum\nolimits_{k=0}^{n-1}L_k^{II}(\tau)u_{n-2}\left(t_k^n\right),L_k^{II}(\tau)=\left[\ln 2+2\sum\nolimits_{p=1}^{n-1}T_p\left(t_k^n\right)T_p(\tau)/p\right]/n \tag{86}$$

- and quadrature formulas for integrals with smooth kernels,

$$K^{I}u_{n-2}(\tau)=\sum\nolimits_{k=0}^{n-2}K_{l,1}^{k(I)}(\tau)u_{n-2}\left(t_{0k}^n\right),K_{l,1}^{k(I)}(\tau)=K_{l,1}\left(\tau,t_{0k}^n\right)\left(1-\left(t_{0k}^n\right)^2\right)/n,l=1,2 \tag{87}$$

$$K^{(II)}u_{n-1}(\tau)=\sum\nolimits_{k=0}^{n-1}K_{m,2}^{k(II)}(\tau)u_{n-1}\left(t_k^n\right),K_{m,2}^{k(II)}(\tau)=K_{m,2}\left(\tau,t_k^n\right)/n,m=1,2 \tag{88}$$

On satisfying the first IE of (71) in the zeros of the second-kind Chebyshev polynomial $\left\{t_{0j}^n\right\}_{j=0}^{n-2}=\left\{\cos(j+1)\pi/n\right\}_{j=0}^{n-2}$ and the second IE in the zeros of the first-kind polynomial $\left\{t_k^n\right\}_{k=0}^{n-1}=\left\{\sqrt{\cos(2k+1)\pi/(2n)}\right\}_{k=0}^{n-1}$ and using the quadrature formulas (80)–(88), we obtain discrete counterpart of (71),

$$C^Mx^M=b^M,M=0,\pm1,\pm2,\ldots, \tag{89}$$

$$x^M=\left(\left\{u_{n-2}^M\left(t_{0k_1}^n\right)\right\}_{k_1=0}^{n-2},\left\{w_{n-1}^M\left(t_{k_2}^n\right)\right\}_{k_2=0}^{n-1}\right)^T, \tag{90}$$

$$b^M=\left(\left\{g_{1,n-2}^M\left(t_{0l_1}^n\right)\right\}_{l_1=0}^{n-2},\left\{g_{1,n-1}^M\left(t_{l_2}^n\right)\right\}_{l_2=0}^{n-1}\right)^T, \tag{91}$$

$$C^M=\begin{pmatrix}C^{(M)11} & C^{(M)12}\\ C^{(M)21} & C^{(M)22}\end{pmatrix}, \tag{92}$$

where the matrix and the right-hand-part elements are given by the expressions

$$C^{(M)11}=\left\{C_{l_1,k_1}^{(M)11}\right\}_{l_1,k_1=0}^{n-2},C^{(M)1\varphi}=\left\{C_{l_1,k_2}^{(M)12}\right\}_{l_1=0,k_2=0}^{n-2,n-1},C^{(M)2\tau}=\left\{C_{l_2,k_1}^{(M)21}\right\}_{l_2=0,k_1=0}^{n-1,n-2},C^{(M)2\varphi}=\left\{C_{l_2,k_2}^{(M)22}\right\}_{l_2,k_2=0}^{n-1}, \tag{93}$$

$$C_{l_1,k_1}^{(M)11}=a_{11}\left(t_{0l_1}^n\right)A_{l_1,k_1}+b_{11}\left(t_{0l_1}^n\right)\Gamma_{l_1,k_1}^{-1(I)}+c_{11}^M\left(t_{0l_1}^n\right)L_{k_1}^I\left(t_{0l_1}^n\right)+K_{1,1}^{k_1(I)}\left(t_{0l_1}^n\right), \tag{94}$$

$$C_{l_1,k_2}^{(M)12}=b_{12}^M\left(t_{0l_1}^n\right)\Gamma_{l_1,k_2}+c_{12}^M\left(t_{0l_1}^n\right)L_{k_2}^{II}\left(t_{0l_1}^n\right)+K_{1,2}^{k_2(II)}\left(t_{0l_1}^n\right), \tag{95}$$

$$C_{l_2,k_1}^{(M)21}=b_{21}^M\left(t_{l_2}^n\right)\Gamma_{l_2,k_1}^{-1(II)}+c_{21}^M\left(t_{l_2}^n\right)L_{k_1}^I\left(t_{l_2}^n\right)+K_{2,1}^{k_1(I)}\left(t_{l_2}^n\right), \tag{96}$$

$$C_{l_2,k_2}^{(M)22}=c_{22}^M\left(t_{l_2}^n\right)L_{k_2}^{II}\left(t_{l_2}^n\right)+K_{2,2}^{k_2(II)}\left(t_{l_2}^n\right), \tag{97}$$

and $u_{n-2}^M(t_0)$ and $w_{n-1}^M(t)$ denote the polynomials of the degrees of $n-2$ and $n-1$, respectively.

Using technique described in [7], we have proved that the set (71) has unique solution in the corresponding Hilbert spaces for each value of parameter M. If the parameterization functions $\rho_0(t)$, $z_0(t)$ are polynomials, then approximate solutions $u_{n-2}^M(t_0), w_{n-1}^M(t)$ converge to the exact solution of (71) for n ∞ with the rate of convergence $1/n$. The near and far fields are readily expressed through $w^M(\tau), u^M(\tau)$.

As an illustration of this approach we consider a paraboloidal reflector with the focal distance f and the diameter D illuminated by the plane electromagnetic wave propagating under the angle γ to the axis of rotation. In this case, the incident field is given by

$$\overrightarrow{E}^0(\rho,\varphi,z)=\overrightarrow{m}e^{-i\left(\overrightarrow{k},\overrightarrow{R}\right)}, \tag{98}$$

where $\overrightarrow{m}=(\cos\gamma,0,-\sin\gamma)$, $\overrightarrow{k}=k(\sin\gamma,0,\cos\gamma)$ and $\overrightarrow{R}=(\rho\cos\varphi,\rho\sin\varphi,z)$. Thus, the Fourier coefficients of the incident electric field components are

$$E_\varphi^{0(M)}=-(Z/2)(-i)^M\left[J_{M-1}(k\rho\sin\gamma)+J_{M+1}(k\rho\sin\gamma)\right]\cos\gamma e^{-ikz\cos\gamma} \tag{99}$$

DOI: 10.1002/jnm

$$E_\tau^{0(M)} = (Z/2)(-i)^M\left\{\left(i\rho'_\tau \cos\gamma[J_{M-1}(k\rho\sin\gamma) - J_{M+1}(k\rho\sin\gamma)] - 2z'_\tau \sin\gamma J_M(k\rho\sin\gamma)\right\}e^{-ikz\cos\gamma}/l_\tau \right. \tag{100}$$

In Figure 12, we show the total electric-field magnitude patterns normalized by $\left|\vec{E}^0\right|$ in two principal planes near a paraboloidal reflector with optimal parameters $f/D = 0.25$ and $D = 10\lambda$, illuminated by a plane electromagnetic wave propagating under the angle of $\gamma = 30^0$ to the axis of rotation. In Figure 13, we show the far-field scattering patterns in the E-plane and H-plane. As one can see, for this configuration of reflector and angle of incidence there is a strong back-reflection and a shift of the focal region in the E-plane.

More numerical results related to the plane-wave scattering by the spherical and paraboloidal PEC reflectors can be found in the contributed papers [35,36].

6. CONCLUSIONS

We have presented essentials of several Nystrom-type numerical techniques used for discretization of IEs with smooth and singular kernels that appear in the simulation of electromagnetic wave scattering and emission by dielectric cylinders, thin material strips and disks and PEC rotationally symmetric zero-thickness reflectors. These techniques provide either algebraic convergence, as for the strip and reflector scattering, or even exponential convergence, as for the thin dielectric disk and dielectric cylinder scattering. They avoid inner products that have to be integrated numerically and hence have very low computational cost. Conventional practical accuracy of three to four digits in the surface-current and near-field computations is achieved with small discretization orders, only slightly larger than the largest electrical dimension of the scatterer. What is also important and attractive, these algorithms are equally efficient and stable in the computations of electrically small (quasi-static) and electrically large (quasi-optic) scatterers. They are invaluable when unconventionally accurate electromagnetic computations are required, which is the case, for instance, with the extremely low-threshold (high Q-factor)

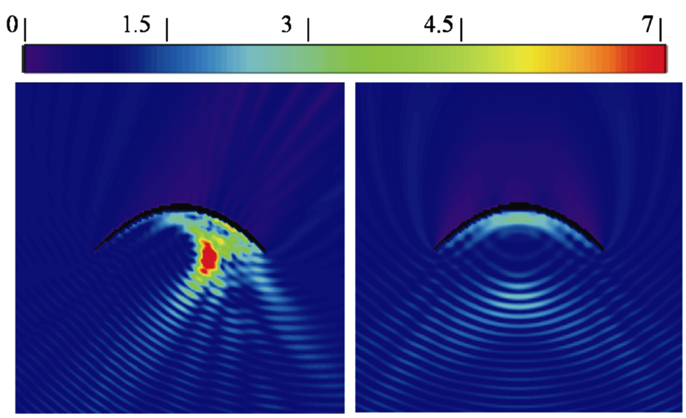

Figure 12. Near-field of the paraboloidal reflector with $f/D = 0.25$, $D = 10\lambda$ illuminated by the plane wave $\gamma = 30°$ in the E-plane (left) and the H-plane (right).

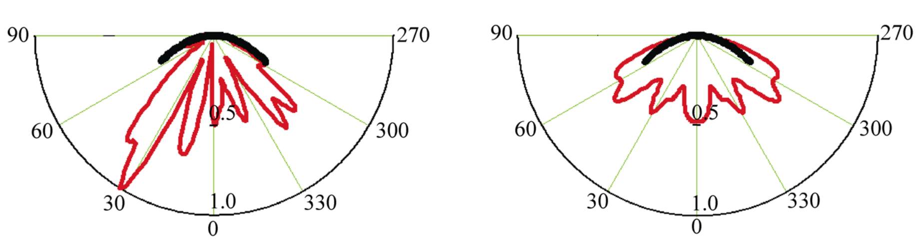

Figure 13. Far-field scattering patterns in the reflection half space for the paraboloidal reflector with $f/D = 0.25$, $D = 10\lambda$ illuminated by the plane wave under the angle of $\gamma = 30°$ E-plane (left) and H-plane (right)

DOI: 10.1002/jnm

whispering-gallery modes of active (passive) dielectric resonators and with multi-element radiatively coupled resonant scatterers.

Thus, Nystrom techniques for solving numerically the IEs of electromagnetics serve as attractive and reliable computational tool. They are quite competitive and sometimes even more economic than the techniques based on MAR. It may appear that the Nystrom techniques eliminate necessity of making analytical regularization or preconditioning of the first-kind singular integral equations. This is true, however, unless one plans to work with iterative numerical algorithms instead of matrix inversion or derive analytical solutions in the form of asymptotic series—in these cases, regularization is necessary.

ACKNOWLEDGEMENTS

This work was supported by the National Academy of Sciences of Ukraine via the State Target Program 'Nanotechnologies and Nanomaterials', the State Agency for Science, Ukraine and the Ministry of Foreign and European Affairs, France via Exchange Program 'Dnipro,' and the European Science Foundation via the Networking Program 'Newfocus'.

REFERENCES

1. Colton D, Kress R. *Integral Equation Methods in Scattering Theory*. Wiley: New York, 1983.
2. Peterson AF. The 'interior resonance' problem associated with surface integral equations of electromagnetics: numerical consequences and a survey of remedies. *Electromagnetics* 1990; **10**:293–312.
3. Valdés F, Andriulli FP, Bagci H, Michielssen E. A Calderón-preconditioned single source combined field integral equation for analyzing scattering from homogeneous penetrable objects. *IEEE Trans. Antenn. Propag.* 2011; **59**(6):2315–2328.
4. Hanson GW, Yakovlev AB. *Operator Theory for Electromagnetics*. Springer-Verlag: New York, 2001.
5. Nosich AI. Method of analytical regularization in wave-scattering and eigenvalue problems: foundations and review of solutions. *IEEE Antenn. Propag. Mag.* 1999; **42**(3):34–49.
6. Nazarchuk ZT. *Numerical Investigation of Wave Diffraction by Cylindrical Structures*. Naukova Dumka: Kyiv, 1989 in Russian.
7. Gandel YV. *Introduction to the Methods of Computation of Singular and Hyper-Singular Integrals*. KhNU Press: Kharkiv, 2001in Russian.
8. Tsalamengas J. Exponentially converging Nystrom's methods for systems of SIEs with applications to open/closed strip or slot-loaded 2-D structures. *IEEE Trans. Antenn. Propag.* 2006; **54**(5):1549–1558.
9. Tsalamengas J. Exponentially converging Nystrom methods in scattering from infinite curved smooth strips. Pt. 2 – TE case. *IEEE Trans. Antenn. Propag* 2010; **58**(10): 3275–3281.
10. Nosich AA, Gandel YV, Magath T, Altintas A. Numerical analysis and synthesis of 2D quasi-optical reflectors and beam waveguides based on an integral-equation approach with Nystrom's discretization. *J. Opt. Soc. Am. A* 2007; **24**(9): 2831–2836.
11. Boriskina SV, Sewell P, Benson TM, Nosich AI. Accurate simulation of 2D optical microcavities with uniquely solvable boundary integral equations and trigonometric Galerkin discretization. *J. Opt. Soc. Am. A* 2004; **21**:393–402.
12. Smotrova EI, Nosich AI. Mathematical study of the 2D lasing problem for the whispering-gallery modes in a circular dielectric microcavity. *Opt. Quant. Electron.* 2004; **36**(1–3):213–221.
13. Smotrova EI, Nosich AI, Benson TM, Sewell P. Cold-cavity thresholds of microdisks with uniform and non-uniform gain: quasi-3D modeling with accurate 2D analysis. *IEEE J. Sel. Top. Quant. Electron.* 2005; **11**(5):1135–1142.
14. Smotrova EI, Byelobrov VO, Benson TM, Sewell P, Ctyroky J, Nosich AI. Optical theorem helps understand thresholds of lasing in microcavities with active regions. *IEEE J. Quant. Electron.* 2011; **47**(1):20–30.
15. Muller C. *Foundations of the Mathematical Theory of Electromagnetic Waves*. Springer: Berlin, 1969.
16. Wang L, Cox JA, Friedman A. Modal analysis of homogeneous optical waveguides by the boundary integral formulation and the Nyström method. *J. Opt. Soc. Am. A* 1998; **15**(1):92–100.
17. Colton D, Kress R. *Inverse Acoustic and Electromagnetic Scattering Theory*. Springer: Berlin, 1998.
18. Abramowitz M, Stegun I. *Handbook of Mathematical Functions*. Nat. Bureau of Standards Publ, Washington DC 1964.
19. Kouznetsov D, Moloney J. Efficiency of pump absorption in double-clad fiber amplifiers. II. Broken circular symmetry. *J. Opt. Soc. Am. B* 2002; **19**(6):1259–1263.
20. Smotrova EI, Benson TM, Sewell P, Ctyroky J, Sauleau R, Nosich AI. Optical fields of the lowest modes in a uniformly active thin sub-wavelength spiral microcavity. *Opt. Lett.* 2009; **34**(24):3773–3775.
21. Smotrova EI, Nosich AI. Simulation of lasing modes in a kite-shaped microcavity laser. Proc. Int. Conf. Advanced Optoelectronics and Lasers (CAOL-10), Sebastopol, 2010; 144–146.
22. Smotrova EI, Nosich AI. Directional light emission from a kite-shaped microcavity laser. Proc. Int. Conf. Transparent Optical Networks (ICTON-11), Stockholm, 2011, We.A4.4.
23. Bleszynski E, Bleszynski M, Jaroszewicz T. Surface-integral equations for electromagnetic scattering from impenetrable and penetrable sheets. *IEEE Antenn. Propag. Mag.* 1993; **35**(6):14–25.
24. Johnson PB, Christy RW. Optical constants of the noble metals. *Phys. Rev. B* 1972; **6**(12):4370–4379.
25. Shapoval OV, Sauleau R, Nosich AI. Numerical algorithm for the scattering by imperfect strips using the Nystrom-type discretization. Proc. Int. Conf. Mathematical Methods in Electromagnetic Theory (MMET*10), Kiev, 2010, IET-3.
26. Shapoval OV, Sauleau R, Nosich AI. Plasmon resonances in the H-wave scattering by a nanosize thin flat silver strip. Proc. Int. Conf. Laser and Fiber-Optic Numerical Modeling (LFNM-10), Sebastopol, 2010, 37–39.
27. Shapoval OV, Sauleau R, Nosich AI. Scattering and absorption of waves by flat material strips analyzed using generalized boundary conditions and Nystrom-type algorithm. *IEEE Trans. Antenn. Propag.* 2011; **59**(9):3339–3346.
28. Balaban MV, Sauleau R, Benson TM, Nosich AI. Dual integral equations

technique in electromagnetic wave scattering by a thin disk. *PIER B* 2009; **16**:107–126.

29. Balaban MV, Sauleau R, Benson TM, Nosich AI. Accurate quantification of the Purcell effect in he presence of a dielectric microdisk of nanoscale thickness. *Micro and Nano Letters* 2011; **6** (6):393–396.
30. Balaban MV, Sauleau R, Nosich AI. Complex-source-point beam scattering by a thin high-contrast dielectric disk. Proc. European Conf. on Antennas and Propagation (EuCAP-11), Rome, 2011, 882–885.
31. Vinogradov SS. Reflectivity of a spherical shield. *Radiophys. Quant. Electron.* 1983; **26**(1):78–88.
32. Davydov AG, Zakharov EV, Pimenov YV. Numerical analysis of fields in the case of electromagnetic excitation of unclosed surfaces. *J. Comm. Tech. Electron.* 2000; **45, no l.2**:247–259.
33. Berthon A, Bills R. Integral equation analysis of radiating structures of revolution. *IEEE Trans. Antenn. Propag.* 1989; **37**(3):159–170.
34. Vasilyev EN. *Excitation of Bodies of Rotation*. Radio i Svyaz: Moscow, 1987(in Russian).
35. VS Bulygin: Interpolation-type numerical method for the electromagnetic wave diffraction by a perfectly conducting axially-symmetric screen, Proc. Int. Conf. Mathematical Methods in Electromagnetic Theory (MMET*10), Kiev, 2010, IET-5.
36. VS Bulygin, AI Nosich, YV Gandel: Near-field focusing and radar cross-section for a PEC paraboloidal screen illuminated by a plane electromagnetic wave, Proc. European Conf. Antennas and Propagation (EuCAP-2011), Rome, 2011, pp. 3836–3840.

AUTHOR'S BIOGRAPHIES

Mikhail V. Balaban was born in Kharkiv, Ukraine. He received the MS degree in Mathematical Modeling from the Kharkiv National University in 2002. He is currently a junior scientist and part-time PhD student of the Institute of Radiophysics and Electronics of National Academy of Science of Ukraine.

His current research interests include singular integral equations, method of analytical regularization, thin disk scatterers, microstrip antennas, eigenvalue problems, plasmon resonances, and lasing.

Elena I. Smotrova was born in Kharkiv, Ukraine. She received the MSc degree in Applied Mathematics from the Kharkiv National University, Kharkiv, in 2002 and the PhD degree in Radiophysics from the Institute of Radiophysics and Electronics (IRE), National Academy of Sciences of Ukraine (NASU), Kharkiv, in 2010. She is currently a scientist at IRE NASU.

Her current research interests include integral equations, eigenvalue problems, and microcavity laser modeling. Dr Smotrova was the recipient of the IEEE Electron Devices Society Graduate Fellowship in 2005 and the IEEE Women in Engineering Region 8 C. Saduwa Award in 2009.

Olga V. Shapoval was born in Nikopol, Ukraine, in 1987. She received the MS degree with honor in Applied Mathematics from Kharkiv National University in 2009. She is currently working toward the PhD degree in Radio Physics at the Laboratory of Micro and Nano Optics, Institute of Radiophysics and Electronics of the National Academy of Science of Ukraine, Kharkiv.

Her current research interests are in the scattering problems by strip-like structures, efficient mathematical and numerical solution techniques, and singular and hyper-singular integral equations. In 2010, she was a recipient of the URSI Young Scientist Award for attending the Asia-Pacific Radio Science Conference in Toyama and the Doctoral Research Award of the IEEE Antennas and Propagation Society.

Vitaliy S. Bulygin was born in 1985 in Kharkiv, Ukraine. He received the MS and PhD degrees in Mathematical Modeling in 2007 and 2010 from the Kharkiv National University and the Institute of Problems of Machine Engineering of the National Academy of Science of Ukraine (NASU), respectively. Since 2010, he has been with the Laboratory of Micro and Nano Optics, Institute of Radiophysics and Electronics, NASU, Kharkiv.

His research interests are in singular and hyper-singular integral equations, numerical methods, reflector and lens antennas, and electromagnetic wave diffraction.

He won the N. I. Akhiyezer Fellowship in 2009 and the Young Scientist Best Paper Prize of the European Microwave Association at MSMW-10 International Symposium, Kharkiv, in 2010.

DOI: 10.1002/jnm

Alexander I. Nosich was born in 1953 in Kharkiv, Ukraine. He received the MS, PhD, and DSc degrees in Radiophysics from the Kharkiv National University, Ukraine, in 1975, 1979, and 1990, respectively.

Since 1979, he has been with the Institute of Radio Physics and Electronics of the National Academy of Science of Ukraine, Kharkiv, where he is currently professor and principal scientist heading the Laboratory of Micro and Nano Optics. Since 1992, he has held a number of guest fellowship and professorship in the EU, Japan, Singapore, and Turkey.

His research interests include the method of analytical regularization, propagation and scattering of waves in open waveguides, simulation of the semiconductor lasers and antennas, and the history of microwaves.

Prof. Nosich was one of the initiators and technical committee chairman of the international conference series on Mathematical Methods in Electromagnetic Theory (MMET). In 1995, he organized IEEE AP-S East Ukraine Chapter, the first one in the former USSR. Currently, he represents Ukraine, Georgia, and Moldova in the European Association on Antennas and Propagation.